

# Extreme enhancement of nonreciprocal wave propagation in magneto-optical metamaterials

Markus Tyboroski <sup>1</sup>, Rair Macêdo <sup>1,2,\*</sup> and Robert E. Camley <sup>1</sup>

<sup>1</sup>*Center for Magnetism and Magnetic Materials, Department of Physics and Energy Science, University of Colorado at Colorado Springs, Colorado Springs, Colorado 80918, USA*

<sup>2</sup>*James Watt School of Engineering, Electronics and Nanoscale Engineering Division, University of Glasgow, Glasgow G12 8QQ, United Kingdom*

 (Received 18 May 2023; revised 12 August 2023; accepted 28 November 2023; published 20 December 2023)

We investigate the magnetic field induced spectral properties of metamaterials incorporating indium antimonide (InSb), using electromagnetic probes in the low terahertz frequency regime. An effective medium theory has been developed to explore the behavior of InSb interspersed with a simple dielectric in a gratinglike structure with various thicknesses and grating filling factors. The metamaterial grating structure impacts the light-matter interactions and substantially modifies reflectivity. Our numerical results demonstrate how nonreciprocal reflection can be enhanced and controlled in this spectral region through the composition of the magnetic grating. The current need for higher frequency communication technology drives the relevancy of this study for application to directional-dependent terahertz devices.

DOI: [10.1103/PhysRevMaterials.7.125201](https://doi.org/10.1103/PhysRevMaterials.7.125201)

## I. INTRODUCTION

Introducing symmetry breaking in materials to obtain directional-dependent wave propagation has become a ubiquitous physical and technological process [1–3]. Whether by inducing spin precession in magnetic materials [1,4] or by inducing cyclotron resonance of current carriers in a solid [5–7], using externally applied magnetic fields is one of the most common ways to achieve said phenomena. For instance, take the second example above of current carriers in two-dimensional electron gases. These are particularly versatile for technological applications as they possess temperature-tunable charge-carrier density but most importantly, in these systems, reversing the wave vector,  $k$ , does not necessarily lead to a wave with the same frequency,  $\omega$ , or simply  $\omega(+k) \neq \omega(-k)$  in the presence of a static applied magnetic field [7]. This is a consequence of the dielectric tensor  $\vec{\epsilon}(\omega)$ , which describes the bulk material, becoming gyrotropic due to the applied magnetic field [8]. Owing to these unusual optical properties, the use of intermetallic structures such as indium antimonide (InSb) is an active area of research [9–11] to achieve nonreciprocal devices including filters and isolators.

It is well known from both experimental and theoretical work in ferromagnets, ferrimagnets, antiferromagnets, and plasmas that a magnetic field oriented parallel to a surface can cause nonreciprocal behavior for surface waves traveling perpendicular to the magnetic field [1,12]. The general

case can be handled by symmetry arguments [1]. This paper deals with how the nonreciprocity can be best seen and utilized.

Most work about nonreciprocity has, in fact, been limited to the low gigahertz frequency range as higher frequencies in ferromagnets and ferrimagnets are difficult to reach with reasonable external fields. So, one motivation for looking at InSb is that the effective mass for the electron in InSb is very small. This means that the cyclotron frequency, given by  $\omega_c = eB/m^*$  can be quite high, in the hundreds of gigahertz, even for relatively small applied fields (an explicit example is provided in Appendixes A and B). The grating allows the electromagnetic wave in an attenuated total reflection (ATR) experiment to couple more effectively to the nonreciprocal surface waves [13], and produces a significant nonreciprocal reflectance.

With the advent of Weyl semimetals [14,15], materials with topologically nontrivial phase of matter, even more rich directional-dependent wave phenomena are being investigated. For example, the waves that propagate at the surface of Weyl semimetals with broken time reversal symmetry are similar to magnetoplasmons in ordinary metals with strong nonreciprocity described by a gyrotropic  $\vec{\epsilon}(\omega)$  [16–18]. As such, these have gained significant interest in the recent past due to their promise for technological applications that require low to no applied magnetic fields. For example, the axion electrodynamics in topological magnetic Weyl semimetals provides a novel and effective mechanism to create nonreciprocal thermal emitters and even to create new scanning tunnelling microscope tips in the form of Veselago lenses for improved imaging [19].

With improvements in the fabrication of advanced artificial materials, engineering structures to display or enhance nonreciprocal phenomena based on magneto-optical effects has become common practice [20]. These include magnetophotonic

\*Rair.Macedo@glasgow.ac.uk

Published by the American Physical Society under the terms of the [Creative Commons Attribution 4.0 International license](https://creativecommons.org/licenses/by/4.0/). Further distribution of this work must maintain attribution to the author(s) and the published article's title, journal citation, and DOI.

metasurfaces [21], hybrid metallic nanostructures [22], and even on-chip magnetoplasmonic nanoantennae [23] for a variety of technological applications ranging from light modulation and sensing to optical wireless communication.

There are several limitations resulting from incorporating these metallic materials in devices. In waveguides, eddy currents lead to significant losses. In optical systems metallic materials lead to uniformly high reflectivity, independent of frequency. By structuring these materials in artificial micro- and nanostructures, eddy currents are significantly reduced and so are losses. Similarly, one can obtain frequency specific reflectivity such as that illustrated in this paper. This provides a strategy for developing high-performance optical devices [24].

Here, we investigate the optical properties of a structured magneto-optical material with primary composition being a magnetized plasma InSb. This material is well known for its terahertz optical properties. In this paper we show that, with a magnetic field present, there is minimal nonreciprocal behavior for both ordinary reflection and ATR from bulk InSb. In contrast, by structuring the InSb into a gratinglike metamaterial, and with ATR, it is possible to significantly enhance the nonreciprocity for a range of frequencies that spans hundreds of gigahertz.

We demonstrate this by calculating the attenuated total reflectance for two geometries and model the material's gyrotropic dielectric tensor  $\vec{\epsilon}(\omega)$  using effective medium theory, which we believe to be an efficient and accurate way to account for the behavior of the overall material. The source of the nonreciprocity is ultimately due to the application of an external static magnetic field. This field, applied in the  $z$  direction, causes the electron movement in the  $xy$  plane to be a curved cyclotron motion. Thus, for example, an  $\mathbf{E}$  field in the  $x$  direction can create motion in the  $y$  direction leading to the off-diagonal components of the permittivity tensor. The off-diagonal components generate the nonreciprocity, with the field setting the cyclotron frequency, as shown explicitly in Appendix A.

One of the main implications of this work is that it offers a consistent and efficient theoretical framework to describe semimetallic structures as a class of materials. For example, the aforementioned nonreciprocal thermal emitters with Weyl semimetals as their primary base component, use the very same type of structuring that we shall discuss throughout this work [16]. Very recently, such structuring was designed in a way that enables near-complete violation of Kirchhoff's law without any external magnetic field, and the behavior of the structure grating was modeled using full-wave simulations using a two-dimensional finite-element solver [18]. In contrast to this extensive calculation an easy-to-use, yet robust, theoretical framework that can be readily employed through  $\vec{\epsilon}(\omega)$  to explain the behavior of these emerging structures—either containing topological quantum materials or simple metallic magneto-optical materials—is highly desirable. The results we present here for the specific material example of InSb, the extreme enhancement of the nonreciprocal effects, offers a pathway for designing nonreciprocal devices for energy harvesting and heat transfer applications through a large band of terahertz frequencies.

## II. RESULTS

As we will demonstrate, the electromagnetic response of InSb is much more interesting when we combine it into a metamaterial grating structure such as that shown in Fig. 1. The InSb bars of width  $d_2$  are separated by a dielectric material of width  $d_1$  and the overall dielectric tensor of the metamaterial can be described using an effective medium method, as detailed in Appendix C. We are interested in transverse magnetic (TM) polarized incident light waves; there are two ways the grating can be structured with respect to the incident radiation: one in which the  $\mathbf{H}$  field of the incident wave is perpendicular to the grooves in the grating [as shown in Fig. 1(a)] and another in which the  $\mathbf{H}$  field is parallel to the grating grooves [see the schematic in Fig. 1(b)]. We chose a TM wave for two reasons: (1) This geometry allows the interaction of the electromagnetic wave with the cyclotron motion and (2) the calculations, though still lengthy, are simpler for this mode as no cross polarization occurs for the reflected or transmitted wave.

To create some context, we start by presenting data for simple reflection off the surface of a single InSb film of thickness  $d = 0.5$  cm on a thick dielectric substrate with  $n = 1.414$  corresponding to  $\epsilon_s = n^2 = 2.0$ . This is shown in Fig. 1(c) as a reflectance color map, i.e., reflectance as a function of both wavenumber,  $\omega/2\pi c$ , and incident angle  $\theta$ . Here, while a magnetic field is present ( $B \approx 0.04$  T), we can see that it does not create any strong nonreciprocity. In fact, for almost all incident angles and frequencies, the film is weakly reflective above  $7.0 \text{ cm}^{-1}$  (or  $0.2$  THz). This is highlighted by the difference between the reflectance for positive and negative incident angles shown in Fig. 1(d), which only shows weak spots (less than 20% difference) for a small range of frequencies around  $20 \text{ cm}^{-1}$ .

It is worth noting that, while not shown here, we have also calculated reflectance for simple reflection off the surface of an effective medium grating metamaterial, again with a thick substrate present, and found that the results do not differ substantially from those shown in Figs. 1(c) and 1(d); in other words, there is no significant nonreciprocity. This remained the case for the whole range of possible filling fractions. For the dielectric medium that fills the grating slits, we used an index of refraction,  $n$ , of 1.414 (same as the substrate). This value is typical of Teflon, which is widely employed in microwave devices [25]. Additional information on parameters and the calculation can be found in Appendix B.

Therefore, simple reflectivity does not turn out to be very interesting, so we now turn our attention to ATR (see Appendix D for full details on the ATR calculation). In particular, we will focus on the Kretschmann configuration [26] shown in Fig. 2(a) where a dielectric prism is placed above the metamaterial that rests on a semi-infinite dielectric substrate. The situation is very different when one examines the ATR reflectivity. A color map for a metamaterial with a filling fraction (dielectric) of  $f_1 = 0.6$ , thickness  $d = 0.5$  cm, and with the  $\mathbf{H}$  field of the incident radiation perpendicular to the grating grooves is shown in Fig. 2(a). The dielectric constant of the prism is  $\epsilon_p = 11$ , typical of a Si prism [27].

Figure 2(b) presents the reflectance map with the cyclotron frequency set to zero, equivalent to  $B = 0.0$  T, showing the

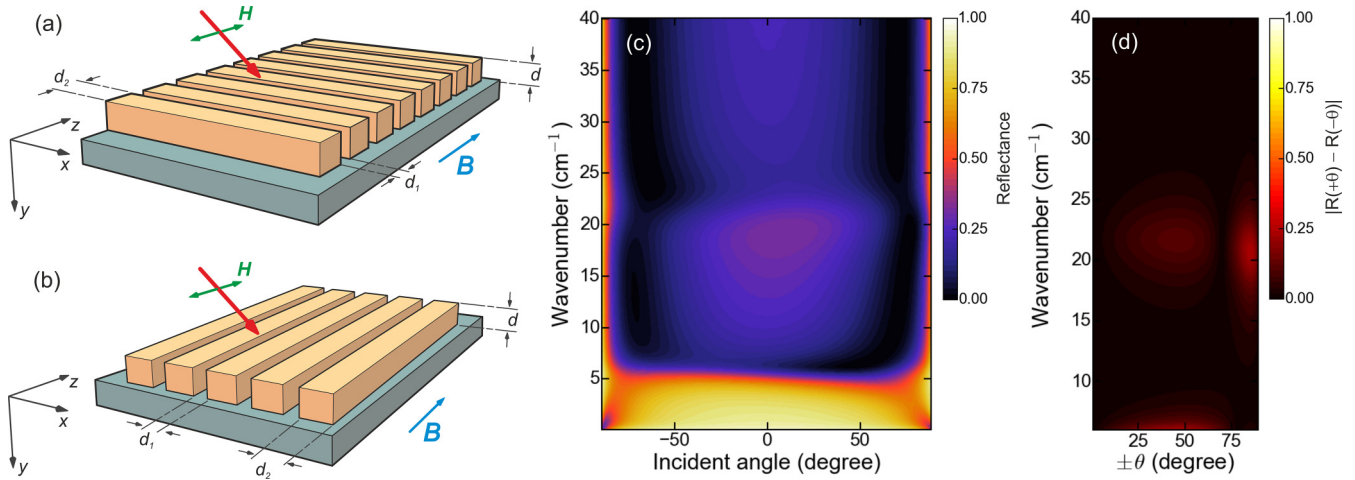


FIG. 1. Schematics illustrating the key geometries used in this paper where we examine the electromagnetic response to a TM wave incident on a grating structure composed of InSb ( $d_2$ ) and a dielectric ( $d_1$ ) with a magnetic field applied in the  $z$  direction for (a) the case where the incident  $\mathbf{H}$  field is perpendicular to the InSb stripes and (b) when the incident  $\mathbf{H}$  field is parallel to the InSb stripes. (c) Reflectance map showing the reflectance as a function of incident angle and wavenumber for a single InSb film of thickness  $d = 0.5$  cm on a substrate of dielectric constant  $\epsilon_s = 2.00$  and an applied field  $B \approx 0.04$  T. (d) Difference  $|R(+\theta) - R(-\theta)|$  between the reflectance for positive and negative incident angles using the data shown in panel (c).

expected symmetric response where positive and negative incident angles give the same response in the absence of an externally applied magnetic field. Figure 2(c) shows a reflectance map with an externally applied magnetic field of  $B \approx 0.04$  T producing a cyclotron frequency at  $\omega_c/2\pi c = 16.7 \text{ cm}^{-1}$  (or 0.5 THz). As in all cases of filling fraction, there is a wide central region of low reflectivity. This region of nonreflective behavior narrows as the filling fraction,  $f_1$ , increases (less InSb in the grating). This can be understood as arising from the change in the effective dielectric constant in the grating region as the filling fractions are changed. We will explore this in more detail below.

The most significant difference between the ATR results and the simple reflectivity is that there is now a dramatic nonreciprocal behavior in the spectrum when comparing positive and negative incident angles. In particular, this behavior becomes more prominent for wavenumbers from 5 to  $25 \text{ cm}^{-1}$  (corresponding to frequencies from 0.15 to 0.75 THz), i.e., frequencies around the cyclotron frequency  $\omega_c$ .

In Fig. 3 we show the reflectance color map for ATR again, but this time for the geometry where the  $\mathbf{H}$  field of the incident radiation is parallel to the grooves in the metamaterial [as shown in Fig. 3(a)]. Again, we use a filling fraction for the dielectric of  $f_1 = 0.6$  and thickness  $d = 0.5$  cm. Figure 3(b) shows the reflectance map with the cyclotron frequency set to zero while Fig. 3(c) shows the case with a nonzero magnetic field ( $B \approx 0.04$  T). Again, there is a wide central region of nonreflectivity that narrows as the filling fraction increases. There is also nonreciprocal behavior between positive and negative incident angles for large incident angles. The most significant nonreciprocity again occurs between 5 and  $25 \text{ cm}^{-1}$ ; however, the shape of the nonreciprocity is somewhat different than that for the parallel configuration and less dramatic especially for lower wavenumbers (here it is mostly localized between 15 and  $20 \text{ cm}^{-1}$ ).

To highlight the extreme enhancement of the nonreciprocity, in Fig. 4 we show the difference between the ATR reflectance spectra for positive and negative angles of incidence ( $|R(+\theta) - R(-\theta)|$ ). We see that ATR enhances the nonreciprocity slightly, even for a single InSb film. In Fig. 4(a) there are some weak regions where nonreciprocity is obtained below  $10 \text{ cm}^{-1}$  and a stronger nonreciprocal region around  $30 \text{ cm}^{-1}$  for very high incident angles. In contrast, when structuring and ATR are introduced, the nonreciprocal features are drastically enhanced across the spectral region shown in Figs. 4(b) and 4(c). When the dielectric grooves in the metamaterial are perpendicular to the  $\mathbf{H}$  field of the incident wave [Fig. 4(b)], not only is the nonreciprocity at low frequencies enhanced to 100% change between  $R(+\theta)$  and  $R(-\theta)$ , but some nonreciprocal features appear throughout the spectral region shown. For the case when the dielectric grooves in the metamaterial are parallel to the  $\mathbf{H}$  field of the incident wave [Fig. 4(c)], a similar enhancement is observed. However, this time, a nonreciprocal region emerges between 15 and  $20 \text{ cm}^{-1}$  for high incident angles, which is in stark contrast to what is observed in the case of a single film shown in Fig. 4(a).

As we have seen, nonreciprocity can be dramatically enhanced when a dielectric grating is incorporated into InSb composing a metamaterial structure. However, the filling factor (or composition of the metamaterial) is not the only way nonreciprocity can be enhanced. This can be combined with the thickness of the metamaterial grating in order to enhance nonreciprocity as well as control the frequencies at which it happens. In Fig. 5 we show the ATR spectra for systems with thinner metamaterial films with  $d = 250 \mu\text{m}$  (0.025 cm) and  $d = 25 \mu\text{m}$  (0.0025 cm) for geometries where the incident beam has its  $\mathbf{H}$  field perpendicular (left column) and parallel (right column) to the grooves.

Once again, we see a central region of low reflectance that is now broken up by bands of somewhat higher reflectance.

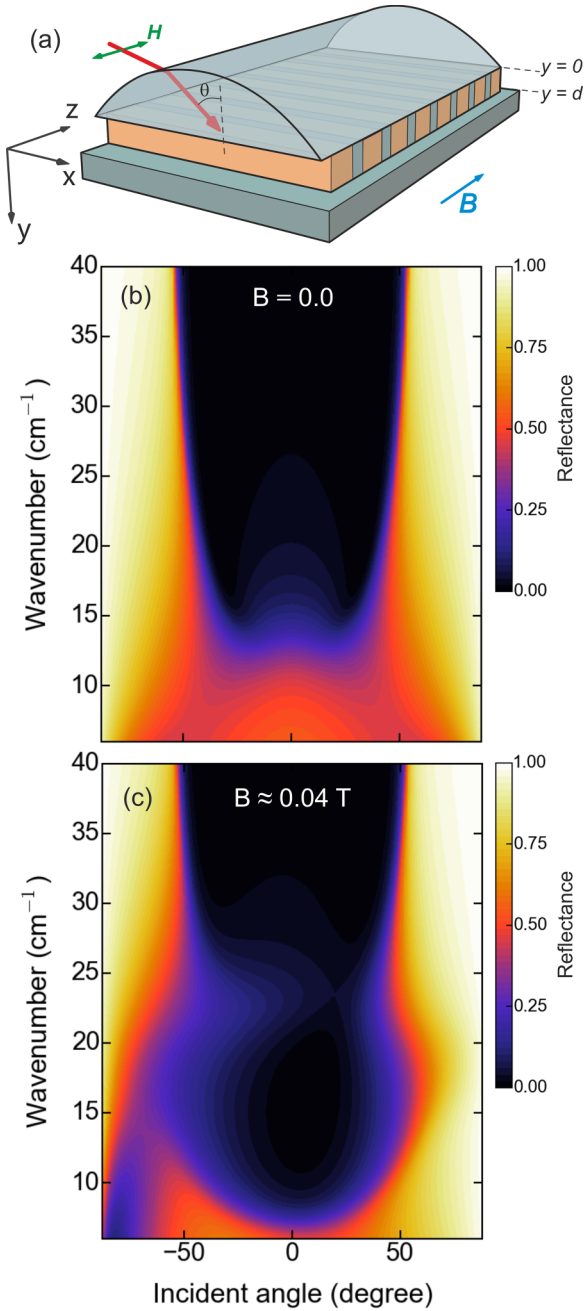


FIG. 2. (a) Kretschmann ATR configuration where the metamaterial sits in between a prism and a thick substrate. The  $\mathbf{H}$  field of the incident wave is perpendicular to the dielectric grooves in the metamaterial. (b) ATR color map showing the reflectance as a function of both incident angle and wavenumber with the cyclotron frequency set equal to zero ( $B = 0.0$ ) and (c) includes a cyclotron frequency of 0.5 THz (corresponding to  $B \approx 0.04 \text{ T}$ ), both for the geometry shown in panel (a). The effective medium film thickness for the metamaterial grating region is  $d = 0.5 \text{ cm}$ , the substrate dielectric constant is  $\epsilon_s = 2.00$ , and the overlayer dielectric constant is  $\epsilon_p = 11.00$ .

For  $d = 250 \mu\text{m}$  [Figs. 5(a) and 5(c)] we find significant nonreciprocity occurs at a similar region to the thicker films, namely, between 5 and 25  $\text{cm}^{-1}$  [as highlighted in Figs. 5(b) and 5(d)]. However, coarse bands of variable behavior are now

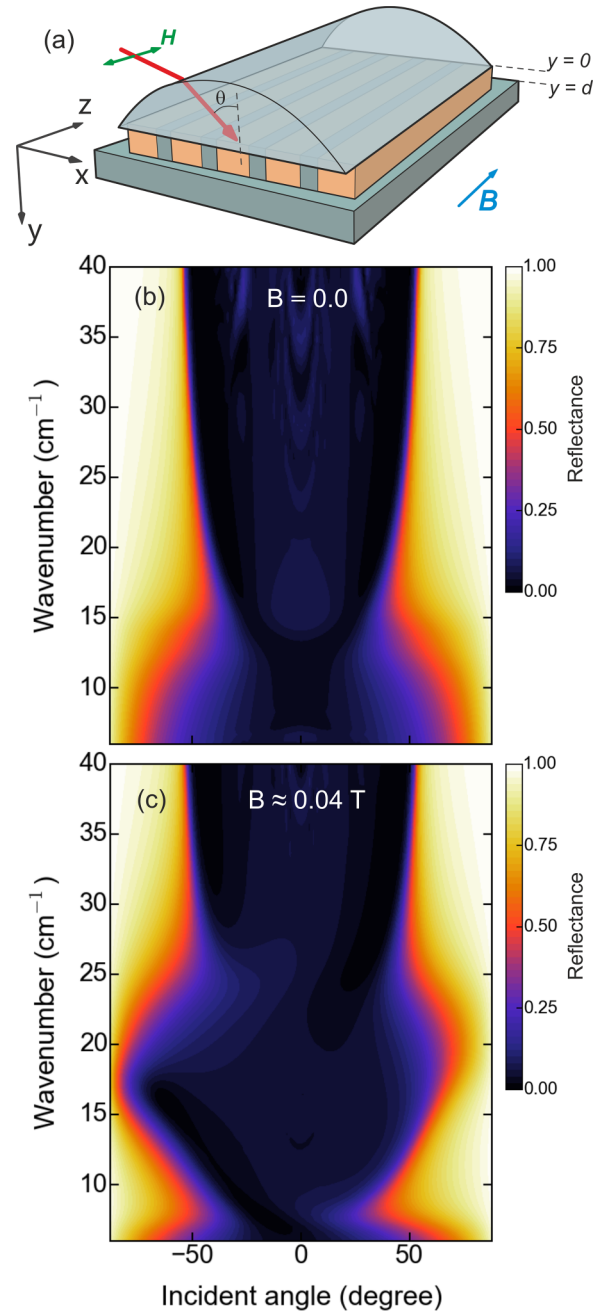


FIG. 3. (a) Kretschmann ATR configuration where the metamaterial sits in between two dielectric layers. The  $\mathbf{H}$  field of the incident wave is parallel to the dielectric grooves in the metamaterial. (b) ATR color map showing the reflectance as a function of both incident angle and wavenumber with the cyclotron frequency set equal to zero ( $B = 0.0$ ) and (c) includes a cyclotron frequency of 0.5 THz (corresponding to  $B \approx 0.04 \text{ T}$ ), both for the geometry shown in panel (a). The effective medium film thickness for the metamaterial grating region is  $d = 0.5 \text{ cm}$ , the substrate dielectric constant is  $\epsilon_s = 2.00$ , and the overlayer dielectric constant is  $\epsilon_p = 11.00$ .

seen, indicating Fabry-Perot resonances [13]. For  $d = 25 \mu\text{m}$  on the other hand, the ATR spectra [Figs. 5(e) and 5(g)] are significantly different compared to the previously examined cases. The thickness is now less than the skin depth in the film, which is  $\sim 68 \mu\text{m}$  for an incident light frequency of

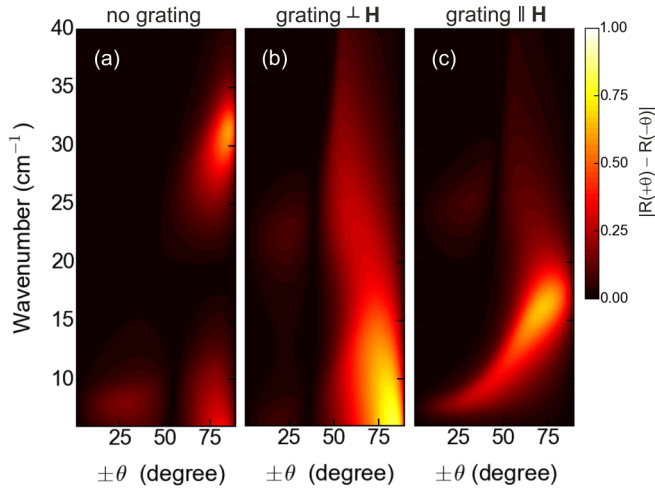


FIG. 4. Difference between the ATR reflectance for positive and negative incident angles comparing the cases of (a) no grating, with the case when the  $\mathbf{H}$  field of the incident wave is (b) perpendicular and (c) parallel to the dielectric grooves in the metamaterial—corresponding to the cases shown in Figs. 2(c) and 3(c).

0.6 THz and for the range of effective media dielectric constant. For this case, and for the geometry where the  $\mathbf{H}$  field is perpendicular to the grating as in Fig. 1(a), there is a strong nonreciprocity but now much more localized between 15 and

25  $\text{cm}^{-1}$  [as highlighted in Fig. 5(f)]. Otherwise, the spectra show highly reflective behavior. In contrast, the geometry where  $\mathbf{H}$  is parallel to the grooves has a weaker nonreciprocity, as seen in Fig. 5(g), but also demonstrates nonreciprocal behavior at lower frequencies, i.e., around 5  $\text{cm}^{-1}$  [as highlighted in Fig. 5(h)].

Now that we have demonstrated that structuring a magneto-optical material can lead to extreme enhancements of the nonreciprocal effects, it is worth exploring the physical reason why this is so. The answer is simple; the grating effectively lowers the overall dielectric constant of the effective medium, allowing total internal reflection to occur at the prism/grating interface. The key point is that pure InSb can have a very large  $\epsilon_{xx}$  and  $\epsilon_{yy}$ , often in the 10–20 range as shown as the solid lines in Fig. 6(a). These values are above the dielectric constant for the Si prism and as a result, electromagnetic waves from the prism goes from a lower index material to a higher index material and there is no critical angle or evanescent wave in the InSb. Thus, the ATR spectra show very little nonreciprocity, as evident in Fig. 6(b).

If we then artificially lower the value of on-diagonal components of the dielectric tensor InSb [dashed lines in Fig. 6(a)] by lowering the background dielectric constant from 15 to 5, the resulting ATR behavior shows a distinct nonreciprocal feature [Fig. 6(c)]; a lowering of the reflectance in the 5 – 20  $\text{cm}^{-1}$  range on for negative incident angles only. While this is an unphysical mechanism, it is an excellent

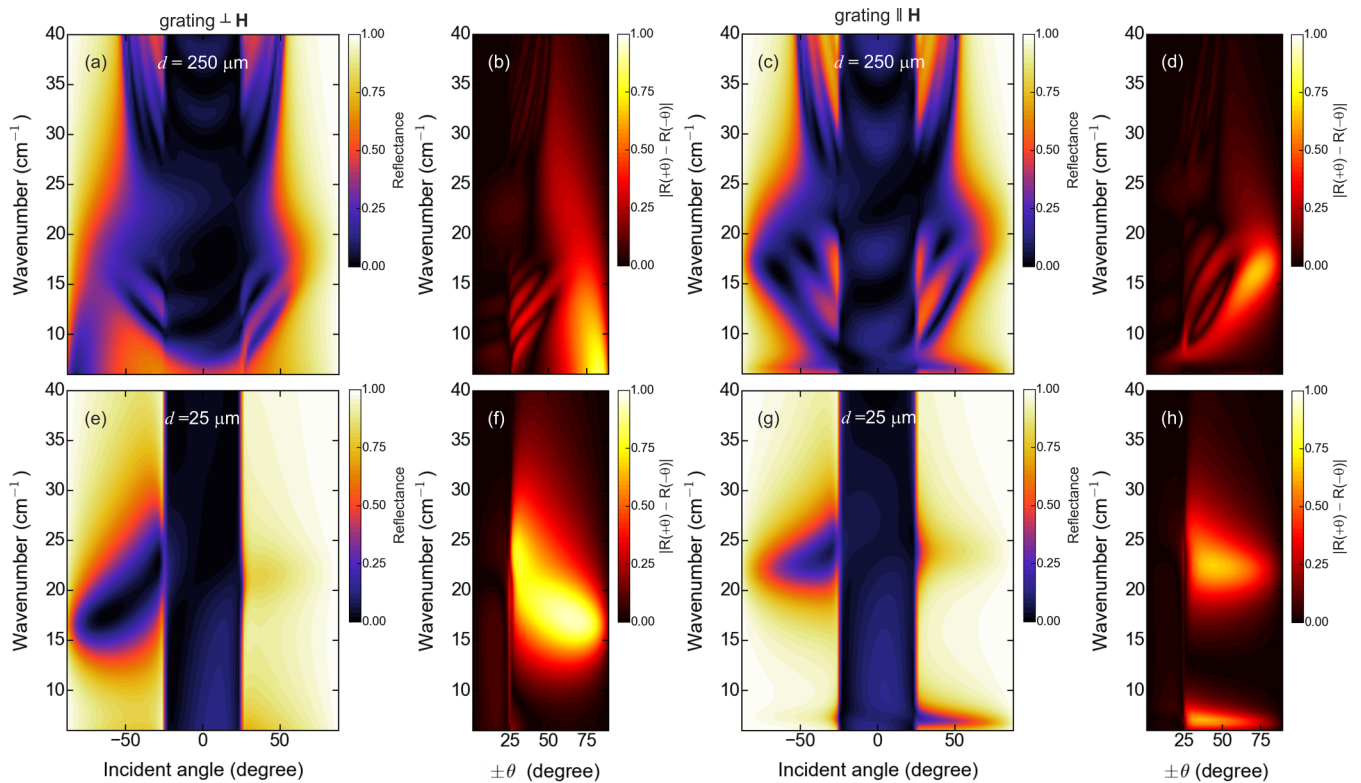


FIG. 5. ATR color maps showing the reflectance as a function of incident angle and frequency for  $d = 250 \mu\text{m}$  and (a)  $\mathbf{H}$  field perpendicular to the grating and (c)  $\mathbf{H}$  field parallel to the grating with respective difference between the reflectance for the positive and negative incident angles given in (b) and (d). Similarly, the ATR maps for (e)  $\mathbf{H}$  field perpendicular to the grating and (g)  $\mathbf{H}$  field parallel to the grating are given for  $d = 25 \mu\text{m}$  with respective difference between the reflectance for the positive and negative incident angles given in (f) and (h). The substrate dielectric constant is  $\epsilon_s = 2.00$  and the overlayer dielectric constant is  $\epsilon_p = 11.00$ .

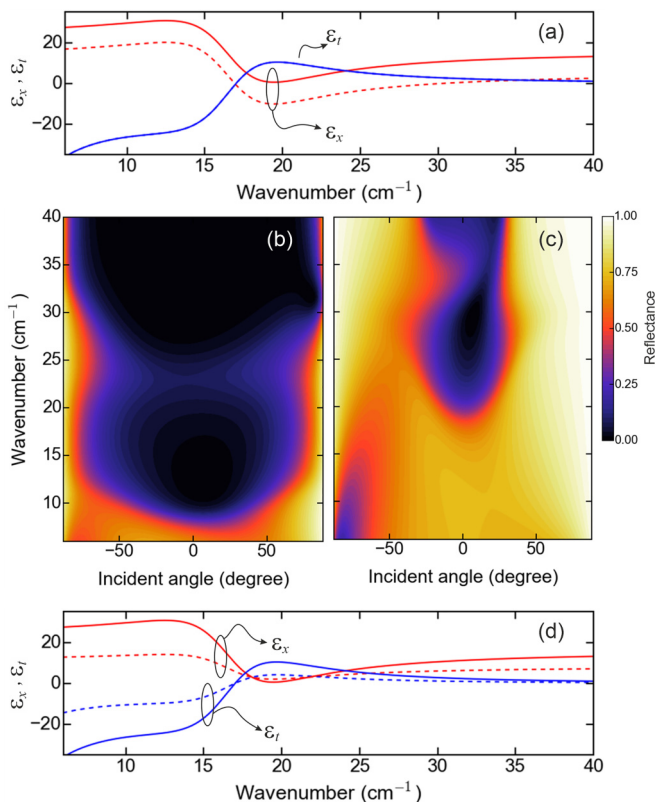


FIG. 6. (a) Dielectric tensor components  $\epsilon_x$  and  $\epsilon_r$  for single InSb with its original background dielectric constant of  $\epsilon_\infty = 15.68$  (solid lines) and lowered at  $\epsilon_\infty = 5.0$  (dashed lines). ATR maps for a single InSb film with (b)  $\epsilon_\infty = 15.68$  and (c)  $\epsilon_\infty = 5.0$ —both using a Si prism with a dielectric constant of  $\epsilon_p = 11$ . (d) Dielectric tensor components  $\epsilon_x$  and  $\epsilon_r$  for a structured metamaterial comprising InSb at  $f_1 = 0.6$  (dashed lines) compared to a single InSb film (solid lines). Note that  $\epsilon_x$  and  $\epsilon_r$  are elements of the effective medium tensor as defined in Appendix C.

demonstration of how lowering the dielectric constant of the material would lead to strong nonreciprocal responses.

With the grating structure, a significant lowering of the effective value of all components of the dielectric tensor of the effective medium is very much possible. In Fig. 6(d), we show the value of the components of the effective dielectric tensor for  $f_1 = 0.6$  (dashed lines) for the  $\mathbf{H}$  field perpendicular to the structuring direction. We compare these with the single-film InSb values (solid lines). Here we see that the values are near or below that of the prism, allowing the creation of evanescent surface waves in the InSb/grating region. These surface waves can be strongly nonreciprocal, leading to a nonreciprocal ATR result discussed throughout this work.

### III. CONCLUSION

Here, we have investigated how structuring a magneto-optical material, such as InSb, can lead to extreme enhancement of nonreciprocal optical responses. We studied two main geometries ( $\mathbf{H}$  field of the incident radiation parallel and perpendicular to the structuring direction) and have focused on the behavior of attenuated total reflection. In addition, we showed how the thickness of the metamaterial can drastically

change the frequencies at which nonreciprocity takes place—finding strongly localized nonreciprocal reflection for thinner films that should be easier to incorporate into optoelectronic devices.

Magneto-optical phenomena of the kind we investigate here has attracted great interest through the decades as it has enabled a series of multifunctional optical devices including isolators, modulators, and even polarizers [28]. A large number of studies in this field have focused on the microwave and communication band, and with the current need for higher frequency communication technology [12,29], we expect our finding to be particularly relevant for directional-dependent terahertz devices [30,31,32]. A significant portion of the current state-of-the-art materials for nonreciprocal propagation in this frequency range suffers from appreciable insertion losses [28]. More recently, on-chip terahertz ultrahigh nonreciprocity has been achieved using InSb, paving the way for integrated nonreciprocal terahertz devices [33]. We expect that our findings could introduce a mechanism through which to obtain broadband nonreciprocity in such devices. Finally, we expect that the effective medium theory we have developed here should be particularly applicable to the newly investigated structures containing symmetry broken semimetals.

### APPENDIX A: DIELECTRIC RESPONSE OF BULK InSb

The dielectric response of InSb for excitations in the terahertz and far-infrared frequency band can be described as a combination of different behaviors [8]. The zero-field, isotropic dielectric function takes the form

$$\epsilon_\infty - \frac{\omega_p^2}{\omega^2 + i\gamma_p\omega} + \epsilon_L.$$

Here,  $\epsilon_\infty$  is a constant that describes the background permittivity (high-frequency absorptions). The second term, also known as the Drude term, describes contributions of free carriers, and the last term  $\epsilon_L$  describes contributions to the permittivity due to lattice vibrations; due to their much higher frequencies, the effects of  $\epsilon_L$  are negligible for the frequency range we investigate here. The constant  $\gamma_p$  is the damping parameter that is typically related to the scattering time  $\tau_p$  by  $\tau_p = 1/\gamma_p$ . The plasma frequency,  $\omega_p$ , is defined as

$$\omega_p^2 = \frac{Ne^2}{\epsilon_0\epsilon_\infty m^*}$$

with  $N$  being the carrier concentration,  $e$  the electron charge,  $\epsilon_0$  the permittivity of free space, and  $m^*$  the effective mass of the charge carriers.

When exposed to an externally applied static magnetic field  $\mathbf{B}$ , the current carriers in InSb are accelerated in spiral orbits about the axis of this field—a phenomenon known as cyclotron resonance with frequency

$$\omega_c = \frac{eB}{m^*}.$$

This external field, and hence cyclotron resonance, introduces anisotropy into the material. In this case, and if we assume that the field is applied in the  $z$  direction, the material's

permittivity tensor takes the form

$$\tilde{\varepsilon}(\omega) = \begin{bmatrix} \varepsilon_{xx} & i\varepsilon_{xy} & 0 \\ i\varepsilon_{yx} & \varepsilon_{yy} & 0 \\ 0 & 0 & \varepsilon_{zz} \end{bmatrix}.$$

Each component can then be written as

$$\varepsilon_{xx} = \varepsilon_{yy} = \varepsilon_{\infty} - \frac{\omega_p^2(\omega^2 + i\gamma_p\omega)}{(\omega^2 + i\gamma_p\omega)^2 - \omega_c^2\omega^2} + \varepsilon_L, \quad (\text{A1})$$

$$\varepsilon_{xy} = -\varepsilon_{yx} = -\frac{\omega_p^2\omega_c\omega}{(\omega^2 + i\gamma_p\omega)^2 - \omega_c^2\omega^2}, \quad (\text{A2})$$

and

$$\varepsilon_{zz} = \varepsilon_{\infty} - \frac{\omega_p^2}{\omega^2 + i\gamma_p\omega} + \varepsilon_L.$$

## APPENDIX B: MATERIAL PARAMETERS

The dielectric constant for InSb varies substantially with temperature or doping. As such, a plasma frequency anywhere between 0.3 [17] and 2.5 THz [28] have been found to be perfectly acceptable parameters. To simplify the results, we chose values typically found near room temperature:  $N = 10^{22} \text{ m}^{-3}$ ,  $m^* = 0.0169m_0$ , and  $\varepsilon_{\infty} = 15.68$ , which yield  $\omega_p/2\pi c = 58 \text{ cm}^{-1}$  (corresponding to 1.74 THz) and a collision frequency of carriers of  $\gamma_p/2\pi c = 3.335 \text{ cm}^{-1}$  (or 0.1 THz [24]). Similarly, the cyclotron frequency can be easily tuned with an externally applied magnetic field  $\mathbf{B}$ . Throughout this work we have taken  $\omega_c/2\pi c = 16.7 \text{ cm}^{-1}$  (or 0.5 THz), which corresponds to  $B \approx 0.04 \text{ T}$ . We note that the small effective mass of the electron in InSb allows relatively modest fields to create nonreciprocity at terahertz frequencies.

## APPENDIX C: STRUCTURED METAMATERIAL: THE EFFECTIVE MEDIUM DIELECTRIC TENSOR

Throughout this work we consider a structured metamaterial, such as the one shown in Fig. 1, where the dielectric material has a of width  $d_1$  and semimetal bars (here we have chosen the example material to be InSb) of width  $d_2$  are separated by the dielectric. We can then regard this structured grating as an effective medium when the period of the one-dimensional structure is smaller than a wavelength or a decay length of the electromagnetic radiation interacting with it [34]. In the effective medium approximation, the structured region is replaced by an effective medium having a permittivity tensor that depends upon the fraction of the material that is dielectric,  $f_1 = \frac{d_1}{d_1+d_2}$ , and the fraction of the material that is semimetal,  $f_2 = \frac{d_2}{d_1+d_2}$ . The effective medium approximation makes use of the assumption that the amplitudes of the  $\mathbf{E}$  and  $\mathbf{H}$  fields do not vary significantly across an individual material. For our choice of materials and frequencies, this requires that the InSb width in the grating be less than 60  $\mu\text{m}$  and the total width of the unit cell be less than 70  $\mu\text{m}$ . This approximation eliminates features that arise from the periodicity of the material including the introduction of band gaps or the shifting of wave vectors by reciprocal lattice vectors. Nonetheless, this approximation can work quite well [35].

In the effective medium method, one constructs an average  $\langle \mathbf{D} \rangle$  and relates it to an average  $\langle \mathbf{E} \rangle$  using electromagnetic boundary conditions. This defines an average permittivity tensor. For this, we start with the definition for  $\langle \mathbf{D} \rangle$  and  $\langle \mathbf{E} \rangle$  as follows:

$$\langle \mathbf{D} \rangle = f_1 \mathbf{D}_a + f_2 \mathbf{D}_b \quad (\text{C1})$$

and

$$\langle \mathbf{E} \rangle = f_1 \mathbf{E}_a + f_2 \mathbf{E}_b. \quad (\text{C2})$$

Since one of the materials composing the effective structure is a simple dielectric, which here we call “material  $a$ ,” its permittivity tensor is a simple scalar, and as such we have

$$\mathbf{D}_a = \varepsilon_a \mathbf{E}_a. \quad (\text{C3})$$

On the other hand, the permittivity for a semimetal such as InSb, which here we call “material  $b$ ,” in the presence of a magnetic field is a tensor. In the presence of a magnetic field, it can be written in a simplified form from that shown in Eqs. (A1) and (A2) as

$$\begin{pmatrix} D_x \\ D_y \end{pmatrix} = \begin{pmatrix} \varepsilon_1 & i\varepsilon_2 \\ -i\varepsilon_2 & \varepsilon_1 \end{pmatrix} \begin{pmatrix} E_x \\ E_y \end{pmatrix}. \quad (\text{C4})$$

We have neglected the  $z$  component as it is not necessary for our calculation. Now use Eqs. (C1) and (C2) to write  $\langle D_x \rangle$  and  $\langle D_y \rangle$  in terms of the  $\mathbf{E}$  values in the different materials. This gives

$$\langle D_x \rangle = f_1 \varepsilon_a E_{xa} + f_2 (\varepsilon_1 E_{xb} + i\varepsilon_2 E_{yb}), \quad (\text{C5})$$

$$\langle D_y \rangle = f_1 \varepsilon_a E_{ya} + f_2 (\varepsilon_1 E_{yb} - i\varepsilon_2 E_{xb}). \quad (\text{C6})$$

We now use the boundary conditions to connect the  $E_x$  and  $E_y$  values in the different materials to the average values. For the structure illustrated in Fig. 1(a), these components of  $\mathbf{E}$  are tangential to the interfaces, which are in the  $xy$  plane, and, in a thin structure, are continuous so one has

$$E_{ya} = E_{yb} = \langle E_y \rangle, \quad (\text{C7})$$

$$E_{xa} = E_{xb} = \langle E_x \rangle. \quad (\text{C8})$$

Now use Eqs. (C7) and (C8) to replace all the  $\mathbf{E}$  values in materials  $a$  and  $b$  with  $\langle \mathbf{E} \rangle$  terms. After some algebra, we obtain the equation that determines the effective medium permittivity tensor.

$$\begin{pmatrix} \langle D_x \rangle \\ \langle D_y \rangle \end{pmatrix} = \begin{pmatrix} f_1 \varepsilon_a + f_2 \varepsilon_1 & i f_2 \varepsilon_2 \\ -i f_2 \varepsilon_2 & f_1 \varepsilon_a + f_2 \varepsilon_1 \end{pmatrix} \begin{pmatrix} \langle E_x \rangle \\ \langle E_y \rangle \end{pmatrix}. \quad (\text{C9})$$

The permittivity tensor appropriate for the geometry in Fig. 1(b) is calculated similarly. One starts with Eqs. (A1)–(C4) again, but now one needs a different set of boundary conditions because the structure is different, i.e., the interfaces are in the  $yz$  plane. In this case the appropriate boundary conditions are that  $D_x$ , the normal component of  $\mathbf{D}$ , and  $E_y$ , the tangential component of  $\mathbf{E}$  are continuous. Using these

conditions, one obtains

$$\begin{pmatrix} \langle D_x \rangle \\ \langle D_y \rangle \end{pmatrix} = \begin{pmatrix} \left(\frac{f_1}{\epsilon_a} + \frac{f_2}{\epsilon_1}\right)^{-1} & if_2 \frac{\epsilon_2}{\epsilon_1} \left(\frac{f_1}{\epsilon_a} + \frac{f_2}{\epsilon_1}\right)^{-1} \\ -if_2 \frac{\epsilon_2}{\epsilon_1} \left(\frac{f_1}{\epsilon_a} + \frac{f_2}{\epsilon_1}\right)^{-1} & \left[ f_1 \epsilon_a + f_2 \left(\epsilon_1 - \frac{\epsilon_2}{\epsilon_1}\right) + \frac{f_2^2 \left(\frac{\epsilon_2}{\epsilon_1}\right)^2}{\left(\frac{f_1}{\epsilon_a} + \frac{f_2}{\epsilon_1}\right)} \right] \end{pmatrix} \begin{pmatrix} \langle E_x \rangle \\ \langle E_y \rangle \end{pmatrix}. \quad (\text{C10})$$

We can represent the dielectric tensor for both geometries in the following way:

$$\vec{\epsilon}(\omega) = \begin{bmatrix} \epsilon_x & i\epsilon_t & 0 \\ -i\epsilon_t & \epsilon_y & 0 \\ 0 & 0 & 1 \end{bmatrix}$$

and we will use this notation in what follows.

#### APPENDIX D: REFLECTANCE AND ATR

As detailed ATR calculations are available in the literature [13,29], we only give a short derivation here, with the most important results. We look for a TM wave, with the oscillating  $\mathbf{H}$  along the  $z$  direction, and the  $\mathbf{E}$  field along  $x$  and  $y$ . Propagation is along  $x$ . The magnetic fields in each region are given by the following equations. In the prism (or air if we are calculating simple reflectivity) the field is

$$\mathbf{H} = e^{i(kx - \omega t)} (A_1 e^{iq_p y} + A_2 e^{-iq_p y}) \hat{z}.$$

Here  $A_1$  is the amplitude of the incident wave and  $A_2$  the amplitude of the reflected wave. In the effective medium the magnetic field has the form

$$\mathbf{H} = e^{i(kx - \omega t)} (A_3 e^{iq_y} + A_4 e^{-iq_y}) \hat{z},$$

and in the semi-infinite substrate, it takes the form

$$\mathbf{H} = e^{i(kx - \omega t)} A_5 e^{iq_s y} \hat{z},$$

where  $A_5$  is the amplitude of the transmitted wave. The electric fields in each region have similar forms and may be derived from the  $\mathbf{H}$  fields using the curl Maxwell equations. For the ATR calculation, we need the  $x$  component of  $\mathbf{E}$  as it will be important in the boundary conditions. We find

$$E_x = e^{i(kx - \omega t)} C_p (A_1 e^{iq_p y} - A_2 e^{-iq_p y}) \quad \text{in the prism,}$$

$$E_x = e^{i(kx - \omega t)} (C_1 A_3 e^{iq_y} - C_2 A_4 e^{-iq_y}) \quad \text{in the effective medium, and}$$

$$E_x = C_s e^{i(kx - \omega t)} A_5 e^{iq_s y} \quad \text{in the substrate.}$$

The coefficients in the equations above are

$$C_p = -\frac{cq_p}{\omega \epsilon_p},$$

which can be evaluated as

$$R = \left| \frac{-C_1 C_2 + C_2 C_p + C_1 C_s - C_p C_s + (C_1 C_2 - C_1 C_p - C_2 C_s + C_p C_s) e^{2idq}}{-C_1 C_2 - C_2 C_p + C_1 C_s + C_p C_s + (C_1 C_2 + C_1 C_p - C_2 C_s - C_p C_s) e^{2idq}} \right|^2.$$

$$C_1 = \frac{(\epsilon_y q + i\epsilon_t k)}{\frac{\omega}{c} (\epsilon_2^2 - \epsilon_x \epsilon_y)},$$

$$C_2 = \frac{(-\epsilon_y q + i\epsilon_t k)}{\frac{\omega}{c} (\epsilon_2^2 - \epsilon_x \epsilon_y)},$$

and

$$C_s = -\frac{cq_s}{\omega \epsilon_s}.$$

The curl equations also give the perpendicular wavevectors in each region in terms of the parallel wavevector,  $k$ , and the frequency,  $\omega$ . These can be written as

$$q_p = \sqrt{\epsilon_p \omega^2 / c^2 - k^2},$$

$$q = \frac{\sqrt{-c^2 k^2 \epsilon_x + \omega^2 \epsilon_x \epsilon_y - \omega^2 \epsilon_t^2}}{c \sqrt{\epsilon_y}},$$

and

$$q_s = \sqrt{\epsilon_s \omega^2 / c^2 - k^2}.$$

The boundary conditions at  $y = 0$ , the interface between the prism and metamaterial grating, are that the tangential components of  $\mathbf{H}$  and  $\mathbf{E}$  are continuous. This gives

$$A_1 + A_2 - A_3 - A_4 = 0$$

and

$$C_p A_1 - C_p A_2 - C_1 A_3 - C_2 A_4 = 0.$$

The same boundary conditions apply at  $y = d$ , the interface between the metamaterial and the substrate, resulting in

$$A_3 \exp(iqd) + A_4 \exp(-iqd) - A_5 \exp(+iq_s d) = 0$$

and

$$C_1 A_3 \exp(iqd) + C_2 A_4 \exp(-iqd) - C_s A_5 \exp(iq_s d) = 0.$$

These four equations allow one to solve for  $A_2$ , the reflected amplitude, in terms of  $A_1$ , the incident amplitude, to find the reflectance

$$R = \left| \frac{A_2}{A_1} \right|^2,$$

As a check on our work, we examined the case where the grating structure is very thin. As the thickness is reduced further to 0.000 01 cm, the reflectance map shows zero reflectance at the Brewster angle (near 23°) and small reflectance for incident angles below the Brewster angle,

rising to a maximum of about 20% at normal incidence. Reflectance for incident angles greater than the critical angle (near 25°) are near 100%. These results are consistent with the usual Fresnel relations for a simple prism/substrate structure.

- 
- [1] R. Camley, Nonreciprocal surface waves, *Surf. Sci. Rep.* **7**, 103 (1987).
- [2] D. Zhao, F. Fan, Z. Tan, H. Wang, and S. Chang, Tunable on-chip terahertz isolator based on nonreciprocal transverse edge spin state of asymmetric magneto-plasmonic waveguide, *Laser Photonics Rev.* **17**, 2200509 (2023).
- [3] L. Feng, M. Ayache, J. Huang, Y.-L. Xu, M.-H. Lu, Y.-F. Chen, Y. Fainman, and A. Scherer, Nonreciprocal light propagation in a silicon photonic circuit, *Science* **333**, 729 (2011).
- [4] R. W. Damon and J. R. Eshbach, Magnetostatic modes of a ferromagnetic slab, *J. Appl. Phys.* **31**, S104 (1960).
- [5] C. L. Hogan, The ferromagnetic Faraday effect at microwave frequencies and its applications, *Rev. Mod. Phys.* **25**, 253 (1953).
- [6] X. Lin, Y. Xu, B. Zhang, R. Hao, H. Chen, and E. Li, Unidirectional surface plasmons in nonreciprocal graphene, *New J. Phys.* **15**, 113003 (2013).
- [7] J. J. Brion, R. F. Wallis, A. Hartstein, and E. Burstein, Theory of surface magnetoplasmons in semiconductors, *Phys. Rev. Lett.* **28**, 1455 (1972).
- [8] J. Dixon and J. Furdyna, Measurement of the static dielectric constant of the InSb lattice via gyrotropic sphere resonances, *Solid State Commun.* **35**, 195 (1980).
- [9] J. Chochol, K. Postava, M. Cada, M. Vanwolleghem, L. Halagacka, J.-F. Lampin, and J. Pistora, Magneto-optical properties of InSb for terahertz applications, *AIP Adv.* **6**, 115021 (2016).
- [10] S. Pakniyat, A. M. Holmes, G. W. Hanson, S. A. H. Gangaraj, M. Antezza, M. G. Silveirinha, S. Jam, and F. Monticone, Nonreciprocal, robust surface plasmon polaritons on gyrotropic interfaces, *IEEE Trans. Antennas Propag.* **68**, 3718 (2020).
- [11] S. Lin, K. Bhattarai, J. Zhou, and D. Talbayev, Giant THz surface plasmon polariton induced by high-index dielectric metasurface, *Sci. Rep.* **7**, 9876 (2017).
- [12] R. Macedo, The 2021 magnetic hyperbolic polaritons roadmap, *Solid State Physics* (Academic, New York, 2021), Vol. 72, Chap. 3, pp. 83–91.
- [13] M. Tyboroski, R. Macedo, and R. E. Camley, Nonreciprocity in millimeter wave devices using a magnetic grating metamaterial, *Phys. Rev. Mater.* **5**, 115201 (2021).
- [14] B. Yan and C. Felser, Topological materials: Weyl semimetals, *Ann. Rev. Condens. Matter Phys.* **8**, 337 (2017).
- [15] A. A. Burkov and L. Balents, Weyl semimetal in a topological insulator multilayer, *Phys. Rev. Lett.* **107**, 127205 (2011).
- [16] B. Zhao, C. Guo, C. A. Garcia, P. Narang, and S. Fan, Axion-field-enabled nonreciprocal thermal radiation in Weyl semimetals, *Nano Lett.* **20**, 1923 (2020).
- [17] D. Wang, B. Yang, W. Gao, H. Jia, Q. Yang, X. Chen, M. Wei, C. Liu, M. Navarro-Cia, J. Han *et al.*, Photonic Weyl points due to broken time-reversal symmetry in magnetized semiconductor, *Nat. Phys.* **15**, 1150 (2019).
- [18] Y. Park, V. S. Asadchy, B. Zhao, C. Guo, J. Wang, and S. Fan, Violating Kirchhoff's law of thermal radiation in semitransparent structures, *ACS Photonics* **8**, 2417 (2021).
- [19] R. D. Y. Hills, A. Kusmartseva, and F. V. Kusmartsev, Current-voltage characteristics of Weyl semimetal semiconducting devices, Veselago lenses, and hyperbolic Dirac phase, *Phys. Rev. B* **95**, 214103 (2017).
- [20] N. Maccaferri, A. Gabbani, F. Pineider, T. Kaihara, T. Tapani, and P. Vavassori, Magnetoplasmonics in confined geometries: Current challenges and future opportunities, *Appl. Phys. Lett.* **122**, 120502 (2023).
- [21] D. O. Ignatyeva, D. M. Krichevsky, V. I. Belotelov, F. Royer, S. Dash, and M. Levy, All-dielectric magneto-photon metasurfaces, *J. Appl. Phys.* **132**, 100902 (2022).
- [22] D. Floess and H. Giessen, Nonreciprocal hybrid magnetoplasmonics, *Rep. Prog. Phys.* **81**, 116401 (2018).
- [23] G. H. Damasceno, W. O. Carvalho, A. Cerqueira Sodre Jr., O. N. Oliveira Jr., and J. R. Mejia-Salazar, Magnetoplasmonic nanoantennas for on-chip reconfigurable optical wireless communications, *ACS Appl. Mater. Interfaces* **15**, 8617 (2023).
- [24] V. Fedotov, Metamaterials, in *Springer Handbook of Electronic and Photonic Materials*, edited by S. Kasap and P. Capper (Springer International Publishing, Cham, 2017), p. 1.
- [25] N. Koizumi, S. Yano, and F. Tsuji, Dielectric properties of polytetrafluoroethylene and tetrafluoroethylene-hexafluoropropylene copolymer, *J. Polymer Sci., Part C: Polym. Symp.* **23**, 499 (1968).
- [26] E. Kretschmann, The determination of the optical constants of metals by excitation of surface plasmons, *Z. Phys. A: Hadrons Nucl.* **241**, 313 (1971).
- [27] R. Macedo and R. E. Camley, Engineering terahertz surface magnon-polaritons in hyperbolic antiferromagnets, *Phys. Rev. B* **99**, 014437 (2019).
- [28] Z. Tan, F. Fan, and S. Chang, Review of terahertz nonreciprocal devices based on gyrotropic material InSb, in *Sixteenth National Conference on Laser Technology and Optoelectronics* (SPIE, Bellingham, WA, 2021), Vol. 11907, pp. 263–274.
- [29] P. M. Yarbrough, K. L. Livesey, R. E. Camley, and R. Macedo, Far-infrared reflection from heterostructures made of ultrathin ferromagnetic layers, *Phys. Rev. Appl.* **12**, 024004 (2019).
- [30] R. Macedo, C. McEleney, M. Gonzalez-Jimenez, and X. Wu, Unidirectional light propagation in natural crystals, *Opt. Photonics News* **31**, 53 (2020).
- [31] X. Wu, C. A. McEleney, Z. Shi, M. Gonzalez-Jimenez, and R. Macedo, Asymmetric reflection induced in reciprocal hyperbolic materials, *ACS Photonics* **9**, 2774 (2022).
- [32] R. Macêdo, T. Dumelow, R. E. Camley, and R. L. Stamps, Oriented asymmetric wave propagation and refraction bending in hyperbolic media, *ACS Photonics* **5**, 5086 (2018).

- [33] S. M. Hanham, A. I. Fernandez-Dominguez, J. H. Teng, S. S. Ang, K. P. Lim, S. F. Yoon, C. Y. Ngo, N. Klein, J. B. Pendry, and S. A. Maier, Broadband terahertz plasmonic response of touching InSb disks, *Adv. Mater.* **24**, OP226 (2012).
- [34] M. H. Tyboroski, N. R. Anderson, and R. E. Camley, An effective medium study of surface plasmon polaritons in nanostructured gratings using attenuated total reflection, *J. Appl. Phys.* **115**, 013104 (2014).
- [35] S. Yuan, L. Chen, Z. Wang, W. Deng, Z. Hou, C. Zhang, Y. Yu, X. Wu, and X. Zhang, On-chip terahertz isolator with ultrahigh isolation ratios, *Nat. Commun.* **12**, 5570 (2021).